APPLIED SCIENCES AND ENGINEERING

Machine embroidery of light-emitting textiles with multicolor electroluminescent threads

Seungse Cho[1]†, Taehoo Chang[2]†, Tianhao Yu[3], Sunland L. Gong[1,4], Chi Hwan Lee[1,2,3]*

Advances in electroluminescent threads, suitable for weaving or knitting, have opened doors for the development of light-emitting textiles, driving growth in the market for flexible and wearable displays. Although direct embroidery of these textiles with custom designs and patterns could offer substantial benefits, the rigorous demands of machine embroidery challenge the integrity of these threads. Here, we present embroiderable multicolor electroluminescent threads—in blue, green, and yellow—that are compatible with standard embroidery machines. These threads can be used to stitch decorative designs onto various consumer fabrics without compromising their wear resistance or light-emitting capabilities. Demonstrations include illuminating specific messages or designs on consumer products and delivering emergency alerts on helmet liners for physical hazards. Our research delivers a comprehensive toolkit for integrating light-emitting textiles into trendy, customized crafts tailored to the unique requirements of diverse flexible and wearable displays.

INTRODUCTION

Light-emitting textiles are gaining increased attention due to their capability to create dynamic and interactive lighting effects, making them suitable for a variety of applications ranging from wearable fashion to health care and to display (*1*–*6*). Traditionally, light-emitting diodes (LEDs) (*7*–*9*) or other types of light sources, such as electroluminescent (EL) thin films (*9*, *10*), have been directly glued or deposited onto garments of interest. However, these approaches can detrimentally affect the inherent fabric properties, such as flexibility, wearability, and washability, and often require difficult conditions, such as high temperatures or vacuum, to be successful. Recent advances of EL threads, which can be woven or knitted, have facilitated the integration of light-emitting textiles on a large scale, spanning up to several meters and incorporating a vast array of lighting lines or pixels (*11*–*16*). Nevertheless, the arrangement of these EL threads is restricted to either straight lines or rectangular patterns because they are interwoven with conductive fibers in both the warp and weft directions. Therefore, there remains a need for a versatile tool that can incorporate light-emitting textiles into fashionable and customized crafts directly on consumer fabric items, with minimal impact on their properties, to suit the specific needs of wide-ranging applications.

Embroidery, which involves stitching strands of threads across the fabric surface, offers a unique ability to create a wide range of decorative designs, from simple to intricate, on any kind of fabric items, making it a craft that is difficult to replicate by knitting or weaving (*17*–*21*). Machine embroidery produces a higher quality stitch and is faster, more precise, and less expensive compared to hand embroidery, thereby facilitating large-scale applications. However, current EL threads are challenged to meet the strict requirements of machine embroidery, such as having a high tensile strength of at least 6 N, a moderate elongation at breakpoint below 100%, and a smooth surface finish (*22*).

Here, we present embroiderable multicolor EL threads, in blue, green, and yellow, that are compatible with universal embroidery machines and can be applied to stitching decorative designs on various consumer fabrics. The EL threads were durable against folding, stretching, and repetitive machine washes while satisfying all the necessary requirements for machine embroidery. In this study, a universal and programmable machine embroidery was used to craft decorative designs (e.g., butterflies, alphabets, stars, and grids) on a variety of consumer fabric items (e.g., cotton towels, flags, t-shirts, and rugs) across large areas up to several tens of centimeters, at a speed exceeding 350 stitches/min. A range of machine-crafted light-emitting textiles were presented, showcasing their utility in pragmatic applications such as displaying messages or designs and functioning as emergency signals for physical hazards.

RESULTS

Embroiderable multicolor EL threads

Figure 1A shows a schematic diagram of the entire process, which covers the production of embroiderable multicolor EL threads and subsequent machine embroidery into light-emitting textiles. The process began by coating an EL layer—a mixture of zinc sulfide (ZnS) phosphors and thermoplastic polyurethane (TPU)—over the surface of a conductive, embroiderable thread (< 0.9 ohms cm^{-1}; Agsis). The coating process occurred in a setup using a household manual winder (Loops & Threads) and tapered nozzle tip (Nordson EFD) (fig. S1), which allowed for a maximum coating rate of approximately 10 cm s^{-1} (movie S1). The EL layer was uniformly applied over the thread in both the longitudinal and circumferential directions, with the ZnS phosphors (average diameter of approximately 20.6 μm) evenly mixed within the TPU (fig. S2A). The thickness of the EL layer was adjusted within a range of 60 to 200 μm by using tapered nozzle tips with different diameters (fig. S2B). For blue, green, and yellow light, doped ZnS phosphors with Cu (~0.1 wt %), Cu (~0.01 wt %), and Mn (~1 wt %) were used, respectively (*23*).

In parallel, a transparent conductive fiber (TCF) was prepared by coating a transparent, embroiderable nylon fiber (300-μm thick; Mandala Crafts Inc.) with silver nanowires (Ag NWs) using an adhesion promoter consisting of a mixture of 90 wt % ethyl acetate and 9 wt % resorcinol (fig. S3A) (*24*). The Ag NWs were chosen for its low electrical

[1]Weldon School of Biomedical Engineering, Purdue University, West Lafayette, IN 47907, USA. [2]School of Materials Engineering, Purdue University, West Lafayette, IN 47907, USA. [3]School of Mechanical Engineering, Purdue University, West Lafayette, IN 47907, USA. [4]Indiana University School of Medicine, Indianapolis, IN 46202, USA.
*Corresponding author. Email: lee2270@purdue.edu
†These authors contributed equally to this work.

resistance, high optical transmittance, and mechanical flexibility (*25*, *26*). The Ag NWs were uniformly coated across the surface of the nylon fiber, forming a conductive and transparent network (fig. S3B). The optical transparency and electrical resistance of the resulting TCF were measured as 83.0 to 90.1% at 550 nm and 73 to 350 ohms with a relative deviation of <5%, respectively (fig. S4B). The TCF maintained against >10,000 cycles of bending at a radius of <1 mm without notable signs of degradation, confirming the adhesion between the nylon fiber and Ag NW network (fig. S4B). To guarantee mechanical durability and antioxidation, a thin layer (<120-μm thick) of a transparent and waterproof fabric sealer (Gorilla Glue Inc.) was used to encapsulate the TCF (fig. S5A). Because the fabric sealer had a high optical transparency (>95% at 550 nm), it rarely affected the EL intensity of the light-emitting pixels (fig. S5B).

Figure 1B displays the EL threads and TCF stitched in an overlapped layout. To create decorative crafts of light-emitting pixels, a universal embroidery machine (b79; Bernette Inc.) was used after stabilizing fabric items and placing them on a stitch plate (fig. S6). The EL threads and TCF were continuously supplied from their respective bobbins. Additional upper thread was then looped around them as they were stitched into a pattern that matched the digital designs. The digital designs were either created by the user or downloaded from a design library.

Figure 1C presents arrays of the blue, green, and yellow light-emitting pixels when subjected to an ac voltage of 120 V at a frequency of 2 kHz. The chromaticity coordinates of the blue, green, and yellow lights were (0.17, 0.45), (0.16, 0.22), and (0.53, 0.42) with respect to the Commission Internationale de l'Éclairage 1931 standard color-matching, respectively (fig. S7A). The relative deviations in emission intensity of the light-emitting pixels in all colors varied by <10%, confirming the uniform formation of pixels through the machine embroidery (fig. S7B). Figure 1D showcases the decorative crafts of light-emitting textiles embroidered on various consumer goods, such as a butterfly on a cotton towel, the letter "P" of Purdue University on a flag, a star on a T-shirt, and a grid on a rug. Even intricate or curved designs can be achieved by selectively illuminating the LED pixels arranged in a rectangular grid. Additional

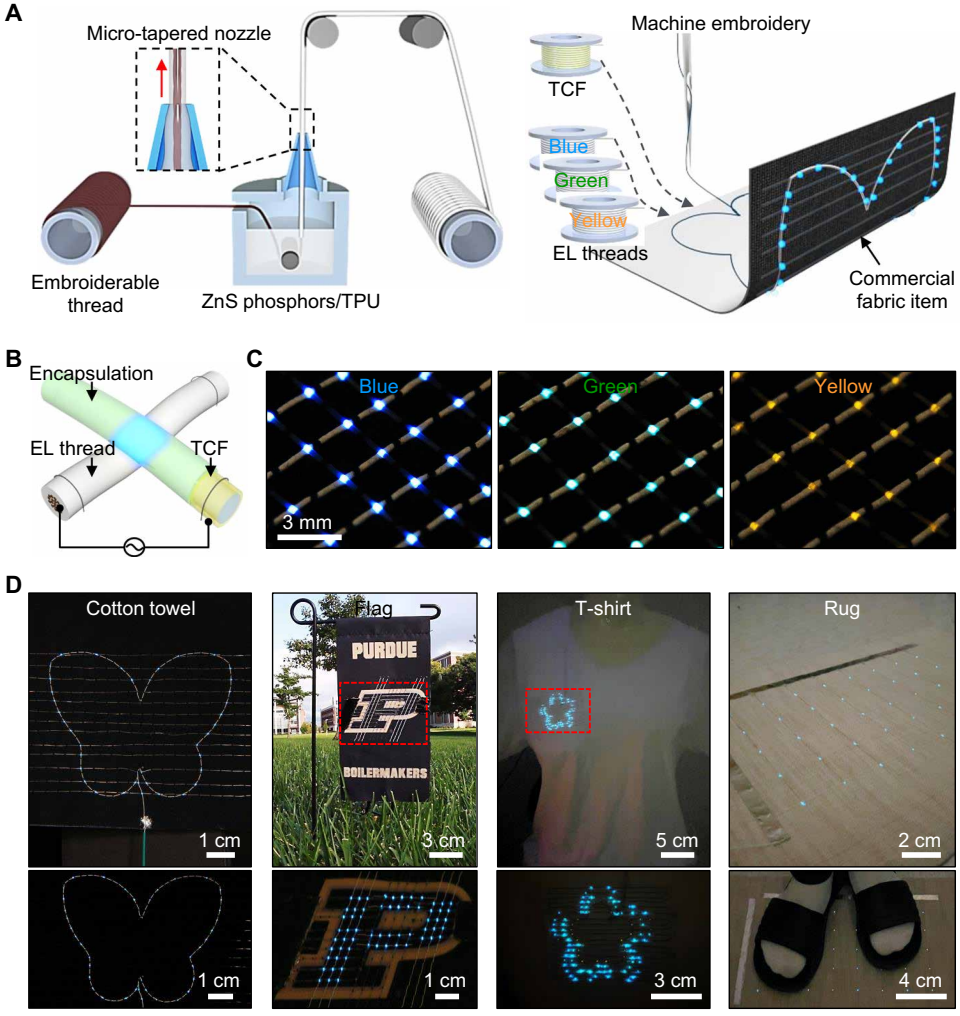

Fig. 1. Embroiderable multicolor EL threads. (**A**) Schematic illustration of producing the EL threads and their subsequent use in machine embroidery for crafting light-emitting textiles. (**B**) Schematic representation of a light-emitting pixel formed at the contact point between the EL thread and transparent conductive fiber (TCF). (**C**) Photographs of the multicolor light-emitting pixel arrays. (**D**) Photographs showcasing the light-emitting textiles embroidered on a cotton towel, flag, t-shirt, and rug.

examples of lighting numbers in green and alphabets in yellow on a cotton towel are shown in fig. S8.

Physical and optical characterizations of EL threads

For machine embroidery, the EL threads must meet specific requirements, such as consistent coverage on the embroiderable thread, a tensile strength of greater than 6 N, moderate elongation at the breaking point of less than 100%, and a surface finish with minimal roughness to avoid stitching jams. Figure 2A shows the measured viscosity of the EL layers, which were prepared using different weight ratios of ZnS phosphors and TPU. The EL layers exhibited the shear-thinning behavior in which their viscosity decreased with an increase of the shear rate. The blue-highlighted region in the graph indicates the viscosity range for producing highly uniform EL layers. When the weight ratio of ZnS phosphors exceeds 5:1 w/w, the EL layers became excessively thick, hindering their consistent production. Figure 2B shows that the diameter of the EL layer increased in a range from ~200 to ~240 μm with respect to increased weight ratio. The cross-sectional views of the EL threads are shown in fig. S9.

Figure 2C presents the tensile strength of the EL threads as compared to that of a plain thread (without the EL layer). The EL threads exhibited a superior tensile strength (σ = 6.7 to 7.3 N) and a slightly lower elastic modulus (E = 17.7 to 21.5 MPa), with a comparable range of elongation at break (ε < 45.6%), compared to a plain thread (σ = 5.7 N, E = 22.7 MPa, and ε = 38.5%). The improved properties of the EL threads can be attributed to the presence of the exceptionally soft and pliant EL layer (E < 0.14 MPa) (fig. S10A). The plain thread, inherently multifilament in nature, exhibits a relaxed demeanor at rest. The introduction of the EL layer acts as an adhesive agent, binding the individual fibers of the thread together, especially when subjected to tension (fig. S10B). The substantial differences in elasticity and pliability between the two adjacent yet distinct materials are the cause of the rise in tensile strength and the decline in elastic modulus, respectively. Figure 2D shows that the surface roughness of the EL threads was as smooth as that of a plain thread (R_q = 7.9 to 8.3 μm), except for the EL threads with a 5:1 w/w ratio (R_q = 15.4 μm). The corresponding measurement data of these properties for the TCF are summarized in figs. 10 (C and D), with values of σ = 51.8 to 54.1 N, E = 90.2 to 90.7 MPa, ε = 13.4 to 13.9%, and R_q = 1.9 μm. Figure 2E demonstrates an increase in the luminance of the EL threads with increasing weight ratio, which reaches a saturation at a 3:1 w/w ratio. The luminance intensity of the EL threads was consistent both along the circumference (Fig. 2F) and in the axial direction (fig. S10E). Taking all of these findings into consideration, both the EL threads with a 3:1 w/w ratio and the TCF are deemed suitable for use in machine embroidery.

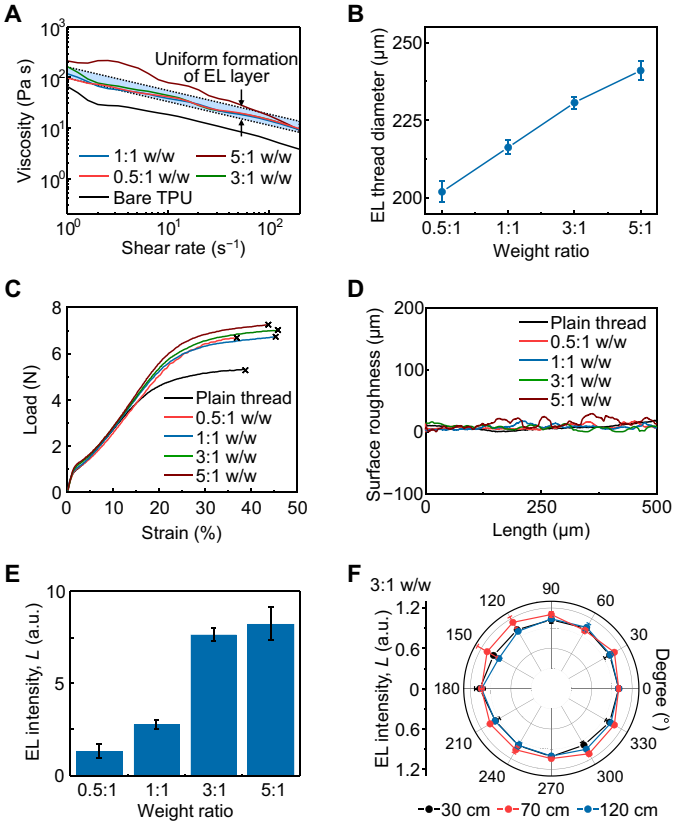

Fig. 2. Physical and optical characterizations of EL threads. (**A**) Shear rate dependence of the viscosity of ZnS phosphor/TPU slurries. (**B**) Weight ratio dependence of thread diameter with respect to ZnS phosphors and TPU. Error bars represent SD, n = 3 for each group. (**C**) Load-strain curves comparison of a plain thread and the EL threads with different weight ratios of ZnS phosphors and TPU. (**D**) Surface roughness comparison of a plain thread and the EL threads with different weight ratios of ZnS phosphors and TPU. (**E**) Weight ratio dependence of EL intensity of the EL threads with respect to ZnS phosphors and TPU. Error bars represent SD, n = 3 for each group. (**F**) Luminance distribution around the circumference of the EL threads. Error bars represent SD, n = 3 for each group. a.u., arbitrary units.

Overall structure and characterizations of light-emitting pixels

Figure 3A presents a schematic illustration (left) and a microscope image (right) of a light-emitting pixel, consisting of the EL thread at the bottom and the TCF at the top, under the application of an ac voltage to emit light. The injected hot carriers in the ZnS phosphors attain high speeds under the influence of an ac electric field and undergo impact ionization. This leads to the radiative relaxation of the luminescent center at a wavelength that corresponds to the dopants in the ZnS lattice, producing light emission at the intersection of the EL thread and the TCF (*5*). Reliable light emission occurred at the intersection even when the EL thread was slid or rotated along the surface of the TCF (movie S2).

Figure 3B displays arrays of light-emitting pixels that were stitched at varying densities, with a stitching distance ranging from 2 to 5 mm (top) and with varying angles (θ) between the EL thread and the TCF, ranging from 15° to 75° (bottom). The relative change in the EL intensity (L/L_0) of the light-emitting pixels remained constant across these cases (Fig. 3C). The L/L_0 of the light-emitting pixels increased exponentially by 54% as the upper thread tension increased from 1.1 to 3.8 N, due to the reduction in the thickness of the EL layer (Fig. 3D). This resulted in a stronger electrical field being applied to the ZnS phosphors. The EL intensity of the light-emitting pixels remained nearly unchanged even after undergoing 100 cycles of pressing at 1.2 MPa and releasing (Fig. 3E). A live streaming demonstration showing the light-emitting pixels on a rug remaining intact even after being repeatedly stepped on and off by an adult with a weight of ~75 kg is presented in movie S3.

Light emission characteristics

Figure 4A illustrates the influence of varying ac voltage (ranging from 25 to 175 V) and frequency (from 2 to 20 kHz) on the EL luminance. With an increase in frequency at fixed voltage of 175 V, the light emission intensity gradually increased, resulting in a luminance increase from 81.38 to 189.2 cd m^{-2}. Above a certain threshold voltage, the probability of electrons being accelerated to excite luminescent centers surged rapidly, leading to a sharp escalation in EL intensity. The experimental data were in good agreement with the fitting curves obtained from the correlation between the EL luminance and the applied voltage at a specific frequency, as described by the following equation

$$L = L_0 \exp(-\beta / V^{1/2}) \quad (1)$$

where L represents the luminance, V represents the applied voltage, and L_0 and β are constants determined by the EL layer (*27*). The current density ranged from 13.6 to 125.1 mA cm^{-2} as the frequency varied from 2 to 20 kHz at a voltage of 175 V (Fig. 4B). The power consumption varied from 1.06 to 76.4 mW as the luminance changed from 81.4 to 189.2 cd m^{-2} at frequencies ranging from 2 to 20 kHz (Fig. 4C). The results confirm its low power consumption, which can be attributed to the alternating field–induced emission mechanism that effectively avoids charge accumulation (*5*, *28*).

Figure 4D shows an 8 × 8 array of light-emitting pixels that maintained stability even when bent, stretched, or rolled, without visible degradation in their emission performance. The L/L_0 of the light-emitting pixels remained under 1.5 and 1.8% even after undergoing repetitive cycles of stretching at 20% (Fig. 4E) and folding in vertical, diagonal, and horizontal directions (Fig. 4F), respectively. Minimal hysteresis was observed in the luminance during these loading-unloading cycles (fig. S11). Real-time streaming of the light-emitting pixels under stretching (beyond 50% until the cotton fabric was damaged) and folding is shown in movie S4.

Figure 4G demonstrates the effect of multiple laundry cycles (>50 cycles) on the L/L_0 of the light-emitting pixels using a standard household washing machine (Amana) and a water-permeable

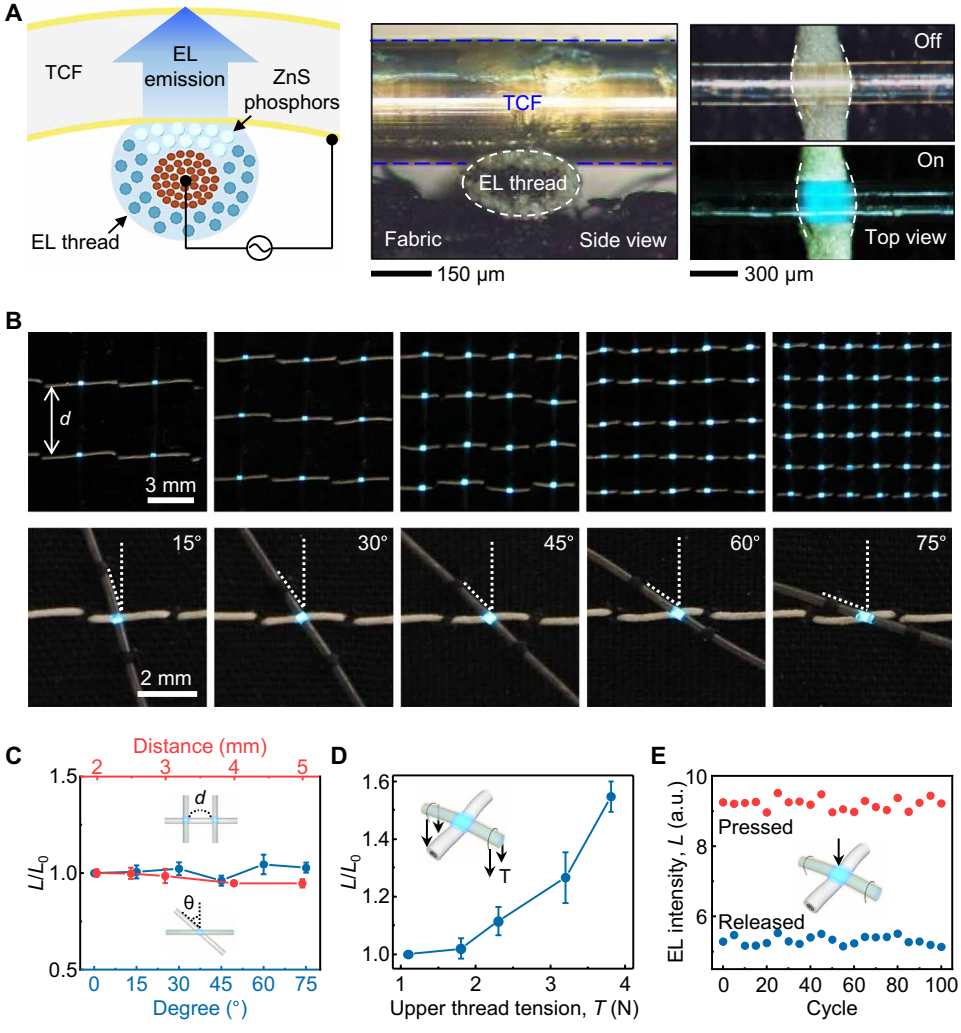

Fig. 3. Overall structure and characterization of light-emitting pixels. (**A**) Schematic representation, side-view, and top-view photographs of a light-emitting pixel created at the point of contact between the EL thread and TCF. (**B**) Photographs of the light-emitting pixels at various stitch distances and angles. (**C**) Relative EL intensity of the light-emitting pixels in relation to the stitch distance and angle between the EL thread and TCF. Error bars represent SD, $n = 3$ for each group. (**D**) Relative EL intensity of the light-emitting pixels as a function of upper thread tension. Error bars represent SD, $n = 3$ for each group. (**E**) Relative EL intensity of the light-emitting pixels under repetitive pressing and releasing cycles.

protective sack. Each washing cycle used a commercial liquid detergent (Tide, 10 ml) in auto-sensing mode, lasting for 45 min, including spinning, rinsing, and spin-drying. After each washing cycle, the light-emitting pixels were dried using an air conditioning heater (PTAC, Amana) at a temperature of 26.7°C for 30 min. The light-emitting pixels showed no noticeable damage when tested with the fabric sealant. In contrast, light-emitting pixels without the fabric sealant became nonfunctional after the first cycle of washing due to loosen contacts between the EL threads and TCF (fig. S12A). Under ambient conditions, the L/L_0 of the light-emitting pixels remained stable for over 3 months without any notable degradation in performance (fig. S12B). However, without the presence of the fabric sealant, the light-emitting pixels deteriorated over time and failed after 1.5 months due to the oxidation of Ag NWs on the TCF surface, which resulted in loss of electrical conductivity (*29*, *30*). Furthermore, the light-emitting pixels exhibited minimal temperature changes (<0.21°C) during continuous operation for over 6 hours at 150 V and 20 kHz, making them suitable for long-term and continuous use (Fig. 4H). The corresponding infrared (IR) images are shown in Fig. 4I.

Proof-of-concept demonstrations

To showcase the capabilities of wearable displays, we embroidered a 6 × 3 array of light-emitting pixels onto a commercial helmet liner for use with a football helmet equipped with an impact sensor. The goal was to detect potential severe head impacts and alert the wearer to the possibility of a concussion. Such wearable displays with real-time warning systems are crucial for preventing and managing traumatic brain injury, particularly in collision sports, where over two million individuals experience concussion annually in the United States (*31*, *32*). They can play a vital role in the early detection and treatment of potential head impacts or concussions, leading to improved outcomes and a reduced risk of further injury or complications.

Figure 5A schematically illustrates the measurement setup that comprises (i) a football helmet (NCAA Replica, Schutt) equipped with an accelerometer (ADXL 377, Adafruit; scan rate, 1 ms), microcontroller (Mega 2560 R3, Arduino), relay (LM2576, Aceirmc), and power supplier (EL inverter, Adafruit); and (ii) a stretchable helmet liner (OutdoorEssentials) with its rear skull cap embroidered with the light-emitting pixels for real-time detection and display of impact direction and severity, respectively. Mechanical impacts were

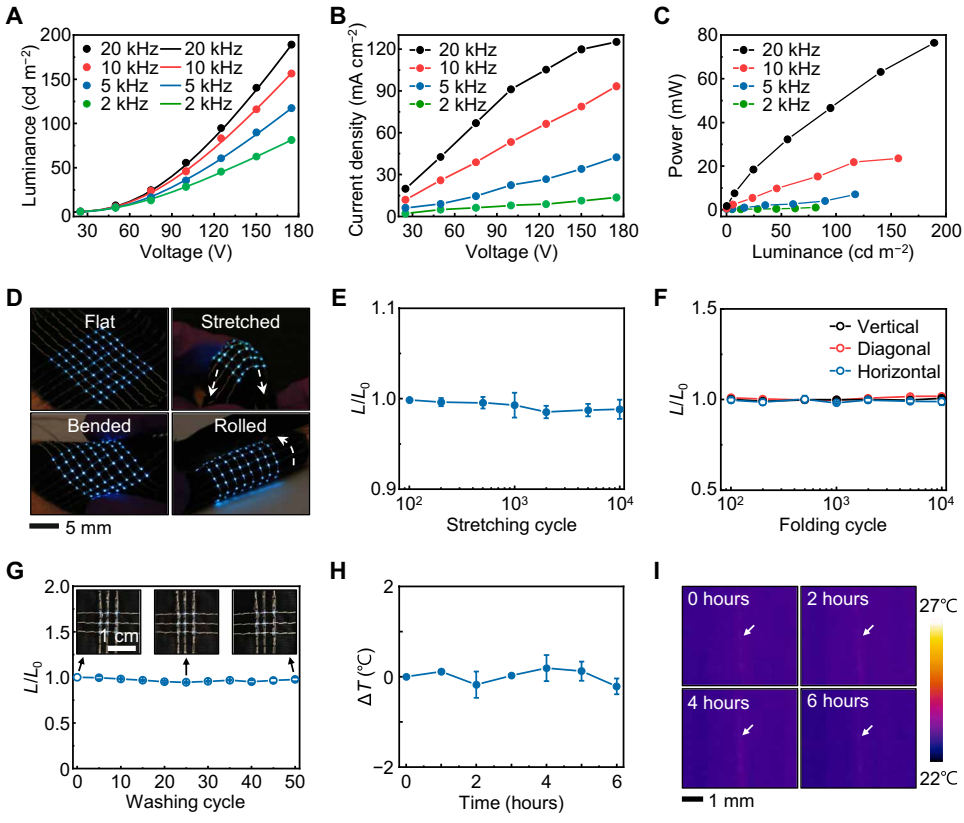

Fig. 4. Light emission characteristics. (**A**) Luminance variation of the light-emitting pixels in response to applied voltages at different frequencies (circles) and corresponding fitting curves (lines). (**B**) Current density of the light-emitting pixels with respect to applied voltages at different frequencies. (**C**) Power consumption of the light-emitting pixels with respect to luminance at different frequencies. (**D**) Photographs of light-emitting textiles under stretching, bending, and rolling. (**E**) Relative EL intensity of the light-emitting pixels during 10,000 stretching cycles at a tensile strain of 20%. Error bars represent SD, $n = 3$ for each group. (**F**) Relative EL intensity of the light-emitting pixels during 10,000 cycles of vertical, diagonal, and horizontal folding. Error bars represent SD, $n = 3$ for each group. (**G**) Relative EL intensity of the light-emitting pixels during multiple laundry cycles. Insets show photographs of the corresponding light-emitting textile. Error bars represent SD, $n = 3$ for each group. (**H**) Local temperature variations of the light-emitting pixels. Error bars represent SD, $n = 3$ for each group. (**I**) Thermal images of the light-emitting pixels after continuous operation up to 6 hours.

applied to a mannequin head using a 13.6 kg dumbbell at various angles and directions, and their severity was classified as mild (10 to 66 g), moderate (66 to 106 g), and severe (>106 g) (*33*).

Figure 5B shows that, when the helmet was affected from the front (θ = 0°, only in the *x* direction), the corresponding row pixels in the *x* column of light-emitting pixels were illuminated depending on the mechanical impact severity. When the helmet was affected from the side oblique (θ = 70°), the corresponding row pixels in both the *x* and *y* columns were illuminated simultaneously. The corresponding results when the helmet was affected from the side (θ = 90°, only in the *y* direction), oblique (θ = 45°), and front oblique (θ = 20°) are shown in fig. S13. Real-time streaming of these demonstrations is shown in movie S5. These demonstrations illustrate a concept for visualizing the mechanical impacts on head in terms of direction, angle, and intensity, which could be valuable for early concussion management in sports or situations where close proximity is necessary in daily life.

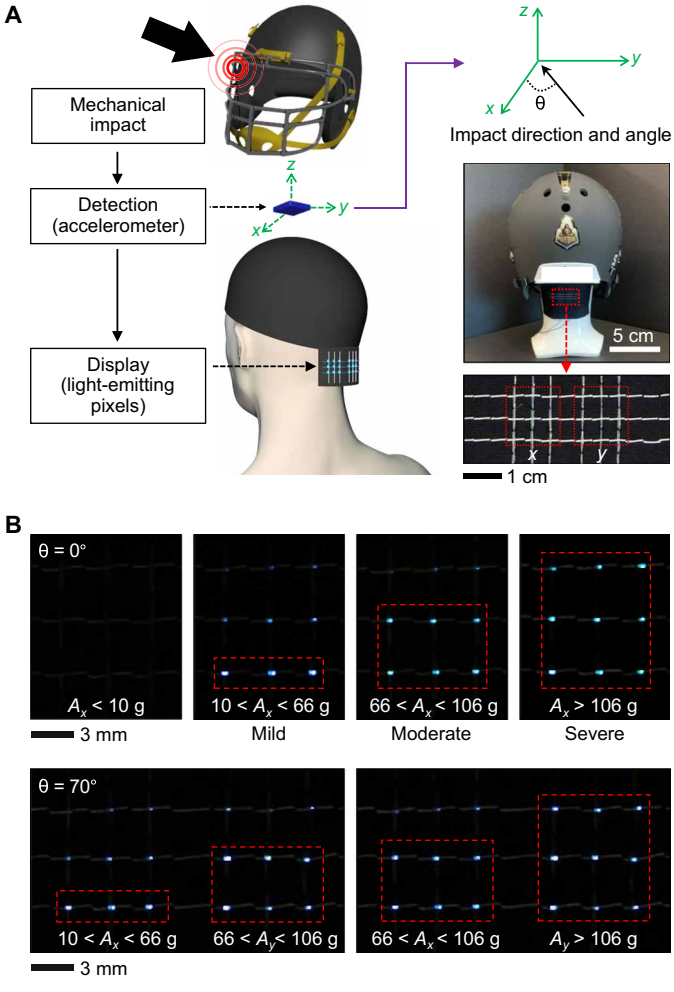

Fig. 5. Proof-of-concept demonstrations. (**A**) Schematic representation of the comprehensive head impact monitoring system, which incorporates a 6 × 3 array of light-emitting pixels into a commercial helmet liner designed for compatibility with a football helmet and includes an integrated impact sensor. (**B**) Photographs of the illuminated light-emitting pixels following an impact in either the *x* direction (θ = 0°) or at an oblique angle (θ = 70°) with varying levels of impact severity (mild, moderate, and severe).

DISCUSSION

In this study, we present a versatile toolkit for crafting light-emitting textiles, which includes multicolor EL threads and TCF that are compatible with standard embroidery machines. Compared to traditional EL threads used for weaving or knitting, these are thinner and more durable, making them suitable for machine embroidery when crafting light-emitting textiles with custom designs. In addition, the EL threads can be embroidered onto a wide range of consumer fabric items up to a meter scale at high speed while ensuring consistent luminescence (relative deviation of <10%), low power consumption (<76 mW), durability (>10,000 cycles of stretching and folding), and machine washability (>50 laundry cycles). Their adjustable colors, luminescent intensities, and pixel positions provide greater versatility and creative potential, allowing them to meet the requirements of a wide range of applications. In light of our proof-of-concept light-emitting textiles, future endeavors should emphasize the integration of safer power mechanisms and enhancement of insulation strategies to bolster both the practicality and safety of wearable applications. Meanwhile, the "ghosting" effect in alternating-current electroluminescent devices is a known phenomenon that can inadvertently activate unwanted pixels, leading to reduced pixel contrast (*34*). However, by using a circuit driver specifically tailored for power supply—where voltage, frequency, and waveforms are meticulously controlled—heightened contrasts in EL pixels can be achieved (*35*). This versatile toolkit for light-emitting textiles can also be used to display real-time measurement results obtained from embedded sensors, making it an ideal solution for health-related applications that require immediate and practical data visualization.

MATERIALS AND METHODS

Fabrication of EL threads

A mixture of tetrahydrofuran (Thermo Fisher Scientific) and *N*,*N*′-dimethylformamide (Thermo Fisher Scientific) was used to dissolve TPU pellets (Elastollan 60A, BASF). The TPU solution was then mixed with commercially available ZnS phosphors with different dopants (Shanghai Keyan Phosphor Technology Co.) using a planetary centrifugal mixer (ARE-310, Thinky) at 2000 rpm for 3 min in weight ratios ranging from 0.5:1 to 5:1. The resulting TPU/ZnS phosphor mixtures were applied onto commercially available Ag-plated conductive threads by passing them through tapered nozzles with different tip diameters of 250, 410, 580, and 840 μm. The EL threads were partially dried in an air-dry oven at room temperature for 5 min after each coating process, which was conducted three times to ensure uniform thickness. To remove residual solvents, the EL threads were then dried overnight at 80°C in an air-dry oven.

Measurement of rheological properties

The viscosity of TPU/ZnS phosphor slurries was measured at room temperature using a rotational rheometer (ARES-G2, TA Instruments, USA) equipped with a standard cone steel with a diameter of 20 mm and an angle of 1°, through a steady-state flow step at a shear rate ranging from 1.0 to 200 s^{-1}.

Fabrication of TCF

The commercially available transparent nylon fibers were subjected to a cleaning process involving sonication in deionized water, acetone, and isopropyl alcohol. To produce hydrophilic surfaces, the cleaned fibers were immersed in a 10 wt % resorcinol solution dispersed in ethyl acetate (Fisher Chemical) and left to dry in a hood for 10 min. The conducting layer was applied by dipping the resorcinol-coated fibers into a 0.25 wt % dispersion of Ag NWs (Flexiowire 2020, SG Flexio Co.). To ensure a reliable and uniform electrical conductivity, the dip-coating process was repeated three times. The resulting TCF was air-dried for 30 min after the dip-coating cycle.

Fabrication of the light-emitting pixels

The light-emitting textiles were produced on consumer fabric items using an embroidery machine (b79, Bernette) loaded with the EL threads and TCFs. Initially, the EL threads were stitched onto a fabric item while adjusting the stitch distance and upper thread tension. Subsequently, the TCF was stitched on the EL threads to form light-emitting pixels at the intersection. To enhance mechanical durability, electrical insulation, and prevent oxidation and, crucially, to ensure washability, a waterproof and transparent sealer (Gorilla Glue Inc.) was applied as an encapsulation layer onto the TCFs and allowed to dry at room temperature. The electrical connection for power supply was established using copper tape and Ag paste.

Characterizations of the light-emitting pixels

Optical photographs of the EL threads, TCFs, and light-emitting pixels were captured using a digital camera (EOS 70D, Canon) equipped with a 67-mm close-up lens (Hoya, Japan), with fixed camera settings (ISO, aperture settings, and shutter speed) unless otherwise specified. The structure of light-emitting pixels was examined using an optical microscope (Eclipse LV150N, Nikon) and field-emission scanning electron microscopy (S-4800, Hitachi, Japan) operated at 5 kV. To measure the electrical properties of the TCF, a sourcemeter (Keithley 2400) and a custom-built LabView code (National Instruments) were used in a two-wire configuration. The transmittance of the TCF was characterized using an ultraviolet-visible spectrophotometer (Cary 50, Varian), scanning the wavelength range of 400 to 800 nm for the TCF film with a thickness of 300 μm (*11*). The luminance of the light-emitting pixels was measured using a chroma meter (CS-200, Konica Minolta, Japan) under an alternating sine voltage supplied by an arbitrary waveform generator (Keithley 3390) connected to a high-voltage power amplifier (9100A-DST, Tabor Electronics). The uniformity of the light-emitting pixels was assessed using the relative deviation (R.D.), which was calculated by R. D. = $[(L_x - L_{avg})/L_{avg}] \times 100$, where L_x is the EL intensity of a single pixel and L_{avg} is the average intensity. All bending, folding, and stretching tests were conducted using a mechanical testing machine (Mark-10, Willrich Precision Instruments). The temperature change of the light-emitting pixels was measured using an IR camera (SC645, FLIR Systems Inc.).

Power consumption calculation

To measure the power consumption of the light-emitting pixels, a test circuit, as shown in fig. S14, was used (*23*). The voltage at specific positions, such as $V_{RMS,BA}$ [the root mean square (RMS), voltage across R_2] and $V_{RMS,A}$ (the RMS voltage across R_1), as well as the resistance of each resistor, were measured using a digital multimeter (Fluke 289, Fluke Corp., USA). The RMS current across each resistor was calculated as $I_{RMS} = V_{RMS}/R$, and the current through resistors 2 and 3 was determined using Kirchoff's current law

$$I_{RMS,2} = \frac{V_{RMS,BA}}{R_2} = I_{RMS,3} \quad (2)$$

By Eq. 2, $V_{RMS,CA}$ (the voltage across the entire test circuit) was calculated

$$V_{RMS,CA} = V_{RMS,CB} + V_{RMS,BA} = V_{RMS,BA}\frac{R_3}{R_2} + V_{RMS,BA} = \left(1 + \frac{R_3}{R_2}\right)V_{RMS,BA} \quad (3)$$

As the current across the first resistor (R_1) equals the total current through the test circuit, the power of the test circuit was calculated using the equation

$$P_{total} = I_{RMS,1} V_{RMS,CA} \cos\theta \quad (4)$$

The phase shift between the current and voltage waveforms across the test circuit, denoted by θ, was measured using an oscilloscope (MSO-X 2024A, Agilent Tech., USA). The power consumption, which includes energy used by a light-emitting pixel and the resistors, was calculated using the equation

$$P_{total} = P_{pixel} + P_{resistors} \quad (5)$$

In conclusion, the power consumption of the light-emitting pixels was obtained by subtracting the power consumption of the resistors, which was calculated using the equation $P = V_{RMS}I_{RMS}$.

Washability test

More than 50 cycles of laundry were carried out using a standard household washing machine (Amana, USA). The light-emitting pixels were put into a water-permeable protective sack. Each laundry cycle was conducted using 10 ml of commercial liquid detergent (Tide, USA) at an auto-sensing mode with a duration of approximately 45 min, which included spinning, rinsing, and spin-drying. After each washing process, the light-emitting pixels were dried for at least 30 min using an air conditioning heater (PTAC, Amana, USA) at 26.7°C. In the machine washability tests, a standard "Amana" household washing machine was used, a methodology corroborated by numerous reputable studies (*7*, *36*–*38*). The significance of international standards such as AATCC LP1-2021 or ISO 105-C06 is recognized, and their incorporation is anticipated for future evaluations to ensure improved reproducibility and validation.

Monitoring of head impact

The light-emitting pixels, arranged in passive matrix arrays, were embroidered onto the rear end of a sports skull cap. This cap was placed on a mannequin head and connected to a microcontroller (Mega 2560 R3, Arduino). An accelerometer (ADXL377, Adafruit, USA) was used to measure the linear acceleration upon head impact. It was positioned inside a commercial football helmet and connected to another microcontroller. This microcontroller drove a relay module, ensuring a controlled voltage power supply for the textile display. A portable external power source (EL wire inverter, Adafruit, USA) was used to provide the necessary energy. The entire system setup is depicted in fig. S15. Whenever the linear acceleration value obtained from the accelerometer (scan rate, 1 ms) exceeded the threshold

values for each impact severity, a voltage signal was generated by the microcontroller and sent to a relay, which turned on the corresponding column and row of the light-emitting pixels.

Supplementary Materials

The PDF file includes:
Figs. S1 to S15
Legends for movies S1 to S5

Other Supplementary Material for this manuscript includes the following:
Movies S1 to S5

REFERENCES AND NOTES

1. Z. Zhang, Light-emitting materials for wearable electronics. *Nat. Rev. Mater.* **7**, 839–840 (2022).
2. G. Chen, X. Xiao, X. Zhao, T. Tat, M. Bick, J. Chen, Electronic textiles for wearable point-of-care systems. *Chem. Rev.* **122**, 3259–3291 (2022).
3. K. Schlingman, Y. Chen, R. S. Carmichael, T. B. Carmichael, 25 years of light-emitting electrochemical cells: A flexible and stretchable perspective. *Adv. Mater.* **33**, e2006863 (2021).
4. L. Wang, X. Fu, J. He, X. Shi, T. Chen, P. Chen, B. Wang, H. Peng, Application challenges in fiber and textile electronics. *Adv. Mater.* **32**, 1901971 (2020).
5. S. Kwon, Y. H. Hwang, M. Nam, H. Chae, H. S. Lee, Y. Jeon, S. Lee, C. Y. Kim, S. Choi, E. G. Jeong, K. C. Choi, Recent progress of fiber shaped lighting devices for smart display applications-a fibertronic perspective. *Adv. Mater.* **32**, e1903488 (2020).
6. Y. Wu, S. S. Mechael, T. B. Carmichael, Wearable e-textiles using a textile-centric design approach. *Acc. Chem. Res.* **54**, 4051–4064 (2021).
7. M. Rein, V. D. Favrod, C. Hou, T. Khudiyev, A. Stolyarov, J. Cox, C.-C. Chung, C. Chhav, M. Ellis, J. Joannopoulos, Y. Fink, Diode fibres for fabric-based optical communications. *Nature* **560**, 214–218 (2018).
8. H. W. Choi, D.-W. Shin, J. Yang, S. Lee, C. Figueiredo, S. Sinopoli, K. Ullrich, P. Jovančić, A. Marrani, R. Momentè, J. Gomes, R. Branquinho, U. Emanuele, H. Lee, S. Y. Bang, S.-M. Jung, S. D. Han, S. Zhan, W. Harden-Chaters, Y.-H. Suh, X.-B. Fan, T. H. Lee, M. Chowdhury, Y. Choi, S. Nicotera, A. Torchia, F. M. Moncunill, V. G. Candel, N. Durães, K. Chang, S. Cho, C.-H. Kim, M. Lucassen, A. Nejim, D. Jiménez, M. Springer, Y.-W. Lee, S. Cha, J. I. Sohn, R. Igreja, K. Song, P. Barquinha, R. Martins, G. A. J. Amaratunga, L. G. Occhipinti, M. Chhowalla, J. M. Kim, Smart textile lighting/display system with multifunctional fibre devices for large scale smart home and IoT applications. *Nat. Commun.* **13**, 814 (2022).
9. E. G. Jeong, Y. Jeon, S. H. Cho, K. C. Choi, Textile-based washable polymer solar cells for optoelectronic modules: Toward self-powered smart clothing. *Energ. Environ. Sci.* **12**, 1878–1889 (2019).
10. Y. Wu, S. S. Mechael, C. Lerma, R. S. Carmichael, T. B. Carmichael, Stretchable ultrasheer fabrics as semitransparent electrodes for wearable light-emitting e-textiles with changeable display patterns. *Matter* **2**, 882–895 (2020).
11. X. Shi, Y. Zuo, P. Zhai, J. Shen, Y. Yang, Z. Gao, M. Liao, J. Wu, J. Wang, X. Xu, Large-area display textiles integrated with functional systems. *Nature* **591**, 240–245 (2021).
12. Z. Zhang, L. Cui, X. Shi, X. Tian, D. Wang, C. Gu, E. Chen, X. Cheng, Y. Xu, Y. Hu, Textile display for electronic and brain-interfaced communications. *Adv. Mater.* **30**, e1800323 (2018).
13. Y. J. Song, J.-W. Kim, H.-E. Cho, Y. H. Son, M. H. Lee, J. Lee, K. C. Choi, S.-M. Lee, Fibertronic organic light-emitting diodes toward fully addressable, environmentally robust, wearable displays. *ACS Nano* **14**, 1133–1140 (2020).
14. Y. H. Hwang, S. Kwon, J. B. Shin, H. Kim, Y. H. Son, H. S. Lee, B. Noh, M. Nam, K. C. Choi, Bright-multicolor, highly efficient, and addressable phosphorescent organic light-emitting fibers: Toward wearable textile information displays. *Adv. Funct. Mater.* **31**, 2009336 (2021).
15. S. Kwon, H. Kim, S. Choi, E. G. Jeong, D. Kim, S. Lee, H. S. Lee, Y. C. Seo, K. C. Choi, Weavable and highly efficient organic light-emitting fibers for wearable electronics: A scalable, low-temperature process. *Nano Lett.* **18**, 347–356 (2018).
16. Y. H. Hwang, B. Noh, J. Lee, H. S. Lee, Y. Park, K. C. Choi, High-performance and reliable white organic light-emitting fibers for truly wearable textile displays. *Adv. Sci.* **9**, 2104855 (2022).
17. R. Lin, H.-J. Kim, S. Achavananthadith, Z. Xiong, J. K. Lee, Y. L. Kong, J. S. Ho, Digitally-embroidered liquid metal electronic textiles for wearable wireless systems. *Nat. Commun.* **13**, 2190 (2022).
18. W. Yang, W. Gong, C. Hou, Y. Su, Y. Guo, W. Zhang, Y. Li, Q. Zhang, H. Wang, All-fiber tribo-ferroelectric synergistic electronics with high thermal-moisture stability and comfortability. *Nat. Commun.* **10**, 5541 (2019).
19. C. Ye, J. Ren, Y. Wang, W. Zhang, C. Qian, J. Han, C. Zhang, K. Jin, M. J. Buehler, D. L. Kaplan, Design and fabrication of silk templated electronic yarns and applications in multifunctional textiles. *Matter* **1**, 1411–1425 (2019).
20. Q. Huang, D. Wang, H. Hu, J. Shang, J. Chang, C. Xie, Y. Yang, X. Lepró, R. H. Baughman, Z. Zheng, Additive functionalization and embroidery for manufacturing wearable and washable textile supercapacitors. *Adv. Funct. Mater.* **30**, 1910541 (2020).
21. M. Sala de Medeiros, D. Chanci, C. Moreno, D. Goswami, R. V. Martinez, Waterproof, breathable, and antibacterial self-powered e-textiles based on omniphobic triboelectric nanogenerators. *Adv. Funct. Mater.* **29**, 1904350 (2019).
22. M. Orth, Defining flexibility and sewability in conductive yarns. *MRS Online Proc. Libr. (OPL)* **736**, D14 (2002).
23. C. Larson, B. Peele, S. Li, S. Robinson, M. Totaro, L. Beccai, B. Mazzolai, R. Shepherd, Highly stretchable electroluminescent skin for optical signaling and tactile sensing. *Science* **351**, 1071–1074 (2016).
24. Y. Atwa, N. Maheshwari, I. A. Goldthorpe, Silver nanowire coated threads for electrically conductive textiles. *J. Mater. Chem. C* **3**, 3908–3912 (2015).
25. Y. Sun, M. Chang, L. Meng, X. Wan, H. Gao, Y. Zhang, K. Zhao, Z. Sun, C. Li, S. Liu, Flexible organic photovoltaics based on water-processed silver nanowire electrodes. *Nat. Electron.* **2**, 513–520 (2019).
26. S. Kang, S. Cho, R. Shanker, H. Lee, J. Park, D.-S. Um, Y. Lee, H. Ko, Transparent and conductive nanomembranes with orthogonal silver nanowire arrays for skin-attachable loudspeakers and microphones. *Sci. Adv.* **4**, eaas8772 (2018).
27. B. Yang, Y. Zhao, M. U. Ali, J. Ji, H. Yan, C. Zhao, Y. Cai, C. Zhang, H. Meng, Asymmetrically enhanced coplanar-electrode electroluminescence for information encryption and ultrahighly stretchable displays. *Adv. Mater.* **34**, e2201342 (2022).
28. Y. Pan, Y. Xia, H. Zhang, J. Qiu, Y. Zheng, Y. Chen, W. Huang, Recent advances in alternating current-driven organic light-emitting devices. *Adv. Mater.* **29**, 1701441 (2017).
29. S. Choi, S. I. Han, D. Jung, H. J. Hwang, C. Lim, S. Bae, O. K. Park, C. M. Tschabrunn, M. Lee, S. Y. Bae, Highly conductive, stretchable and biocompatible Ag-Au core-sheath nanowire composite for wearable and implantable bioelectronics. *Nat. Nanotechnol.* **13**, 1048–1056 (2018).
30. W. Xiong, H. Liu, Y. Chen, M. Zheng, Y. Zhao, X. Kong, Y. Wang, X. Zhang, X. Kong, P. Wang, Highly conductive, air-stable silver nanowire@iongel composite films toward flexible transparent electrodes. *Adv. Mater.* **28**, 7167–7172 (2016).
31. R. Mannix, W. P. Meehan III, A. Pascual-Leone, Sports-related concussions - media, science and policy. *Nat. Rev. Neurol.* **12**, 486–490 (2016).
32. A. J. Carman, R. Ferguson, R. Cantu, R. D. Comstock, P. A. Dacks, S. T. DeKosky, S. Gandy, J. Gilbert, C. Gilliland, G. Gioia, Mind the gaps-advancing research into short-term and long-term neuropsychological outcomes of youth sports-related concussions. *Nat. Rev. Neurol.* **11**, 230–244 (2015).
33. D. King, P. A. Hume, M. Brughelli, C. Gissane, Instrumented mouthguard acceleration analyses for head impacts in amateur rugby union players over a season of matches. *Am. J. Sport Med.* **43**, 614–624 (2015).
34. O. Amiraslanov, P. Lukowicz, J. Cheng, "Large scale, flexible electroluminescent display" in *Proceedings of the 2016 ACM International Joint Conference on Pervasive and Ubiquitous Computing: Adjunct* (Association for Computing Machinery, 2016), pp. 245–248.
35. A. Ivanov, "A printed electroluminescent matrix display: Implementation details and technical solutions" in *2018 IMAPS Nordic Conference on Microelectronics Packaging (NordPac)* (IEEE, 2018), pp. 86–94.
36. T. Chang, S. Akin, M. K. Kim, L. Murray, B. Kim, S. Cho, S. Huh, S. Teke, L. Couetil, M. B. G. Jun, A programmable dual-regime spray for large-scale and custom-designed electronic textiles. *Adv. Mater.* **34**, e2108021 (2022).
37. C. Dong, A. Leber, T. Das Gupta, R. Chandran, M. Volpi, Y. Qu, T. Nguyen-Dang, N. Bartolomei, W. Yan, F. Sorin, High-efficiency super-elastic liquid metal based triboelectric fibers and textiles. *Nat. Commun.* **11**, 3537 (2020).
38. S. Afroj, S. Tan, A. M. Abdelkader, K. S. Novoselov, N. Karim, Highly conductive, scalable, and machine washable graphene-based E-textiles for multifunctional wearable electronic applications. *Adv. Funct. Mater.* **30**, 2000293 (2020).

Acknowledgments
Funding: C.H.L. acknowledges funding supports from the Leslie A. Geddes Endowment at Purdue University. **Author contributions:** Conceptualization: S.C., T.C., and C.H.L. Methodology: S.C. and T.C. Investigation: S.C., T.C., T.Y., S.L.G., and C.H.L. Visualization: S.C. Supervision: C.H.L. Writing—original draft: S.C., T.C., T.Y., S.L.G., and C.H.L. Writing—review and editing: S.C., T.C., T.Y., S.L.G., and C.H.L. **Competing interests:** The authors declare that they have no competing interests. A patent application (serial number: 70259) related to the embroiderable threads was submitted on 25 April 2023 to the Office of Technology Center at Purdue University. The patent is now pending. S.C and C.H.L. are also listed as authors on the patent application. **Data and materials availability:** All data needed to evaluate the conclusions in the paper are present in the paper and/or the Supplementary Materials.

Submitted 22 August 2023
Accepted 1 December 2023
Published 3 January 2024
10.1126/sciadv.adk4295

ScienceAdvances

Machine embroidery of light-emitting textiles with multicolor electroluminescent threads

Seungse Cho, Taehoo Chang, Tianhao Yu, Sunland L. Gong, and Chi Hwan Lee

Sci. Adv. **10** (1), eadk4295. DOI: 10.1126/sciadv.adk4295

Science Advances (ISSN 2375-2548) is published by the American Association for the Advancement of Science. 1200 New York Avenue NW, Washington, DC 20005. The title *Science Advances* is a registered trademark of AAAS.